

Crossover from diffusive to ballistic transport in semiconductor nanostructures

Dan Csontos* and Sergio E. Ulloa

Department of Physics and Astronomy, and Nanoscale and Quantum Phenomena Institute, Ohio University, Athens, Ohio 45701-2979

We present a detailed microscopic study of quasi-ballistic transport in deep submicron semiconductor channels. In particular, we study the crossover between the diffusive and ballistic regimes of transport and identify signatures in the electrostatic response, electron density, and nonequilibrium electron distribution function that are due to ballistic and diffusive transport, respectively. Our theoretical and computational approach is based on the Boltzmann transport equation for a nondegenerate electron system, together with the Poisson equation, from which we obtain the nonequilibrium electron distribution in a self-consistent way. We find that the electron distribution is significantly different from a near-equilibrium, shifted Maxwell-Boltzmann distribution function, and that it displays a large broadening, as well as pronounced features, peaks and shoulders in the high-velocity tail of the distribution. These features are signatures of the nonequilibrium and quasi-ballistic nature of the electron transport. An analysis of the spatial density distributions of electrons in the semiconductor channel region shows that the relative scattering efficiency varies within the channel region. Our study of the crossover between the diffusive and ballistic regimes of transport, which we investigate by downscaling the size of the semiconductor channel, shows that a crossover occurs around a channel length specific to the material parameters, and is clearly accompanied by a redistribution of the voltage drop between the contacts and the channel region. For these transition channel lengths, we also observe clear signatures of the diffusive-to-ballistic crossover in the spatial electron density distribution that manifest as exponential-like and linear spatial dependences, indicative of diffusive and ballistic transport, respectively.

PACS numbers: 73.23.Ad, 72.15.Lh, 72.20.Ht, 73.40.Kp

I. INTRODUCTION

Advances in fabrication and processing of semiconductor materials on the nanoscale are presently enabling the realization of deep submicron and nanoscale semiconductor structures and devices. At these ultrasmall length scales, finite size effects, hot-electrons, ballistic transport and microscopic doping variations are important in determining transport properties. In addition, these systems can be very easily brought out-of-equilibrium, as very high fields are established even for low applied bias voltages.

The physics of electron transport in ultrasmall semiconductor systems is thus very rich as well as complex. Drift-diffusion approaches as well as approximations based on a drifted-Maxwell-Boltzmann distribution break down and an adequate treatment of the nonequilibrium distribution function is needed. In particular, the high-energy tail of the distribution can have complex features that are determined by the scattering processes and the electrostatics within the systems as shown experimentally in Raman spectroscopy measurements of the electron distribution in submicron, inhomogeneous III-V systems.¹ These experiments have shown far-from-equilibrium features such as strongly broadened velocity distributions and interesting high-velocity tail structure.¹

Theoretically, there have been a few recent works that have shown that high-velocity structure in the distribution function can be attributed to ballistic effects.^{2,3,4,5,6,7,8,9,10,11} In a recent paper by us,² we discussed the spatial dependence of the distribution function in deep submicron GaAs channels and showed how

quasi-ballistic signatures manifest as a broadening and high-velocity tail structure, as seen in the experiments. We also analyzed microscopic features of scattering in the channel region in the presence of energy-dependent scattering due to polar-optical phonons. Interesting similar analyses with or without the inclusion of finite scattering have also been previously reported within the same theoretical frameworks.^{3,4,5}

The scattering problem in submicron and nanoscale channels is complicated since scattering and the electrostatic response of the system constitute a strongly coupled physical problem that creates a self-consistent feedback and an interesting charge redistribution. Since pure ballistic transport is not attainable at room temperature in the presence of finite scattering^{3,4} and thus, the transport in submicron systems is quasi-ballistic to a varying degree, it is interesting to ask: What are the signatures of nonequilibrium and quasi-ballistic transport in quantities other than the electron distribution, such as electron density, potential energy and how can one separate the ballistic contribution to the problem and study its influence on the total quantities? More importantly, what constitutes the crossover between diffusive and quasi-ballistic transport and how does it manifest on a microscopic level?

In this paper we report on a detailed study of the crossover between the diffusive and quasi-ballistic regimes of transport in (sub)micrometer scale semiconductor channels, in particular investigating how this crossover manifests in the electrostatic response of the system, the electron redistribution within the channel region, the contribution of ballistic electrons to the total electron density, and the nonequilibrium electron distribution function. Our theoretical and computational

framework is based on a self-consistent solution of the Boltzmann and Poisson equations,¹² which enables us to calculate nonequilibrium electron distributions and corresponding moments, as well as the accurate electrostatic response.

We identify that, for the GaAs system that we study, with a given doping profile and at room-temperature, a crossover to quasi-ballistic transport occurs for channel lengths smaller than $\approx 1.5 \mu\text{m}$. In the electrostatics, the crossover manifests as a redistribution of the potential drop from the channel to the contact regions, for decreasing channel lengths. In the electron density, which we study by separating components with different velocity, we observe interesting spatial dependences reflecting the diffusive-to-ballistic crossover. Finally, on a microscopic level, we examine the nonequilibrium electron distribution function and its phase-space dependence around the crossover regime. The presented results provide insight into the role of scattering, ballistic transport and electrostatics in the transport properties of deep submicron and nanoscale semiconductor systems.

The paper is organized as follows: First, we give a brief introduction to the theoretical model in Section II, referring the reader to Ref. 12 for further details. Next, we will present our results and discussion, first presenting an introduction to the basic signatures of quasi-ballistic transport in Section III A. Subsequently, we discuss the crossover between the diffusive and quasi-ballistic regimes of transport in Section III B. We conclude and summarize our main results in Section IV.

II. MODEL

A microscopic study of the kinetics of quasi-ballistic transport in ultra-small inhomogeneous semiconductor structures requires in principle the solution of the Boltzmann transport equation (BTE). In addition, in order to capture the full physical picture, the BTE needs to be solved self-consistently with the Poisson equation. This is a very difficult task since the BTE is a non-linear, integro-differential equation for the semiclassical distribution function, $f(\mathbf{r}, \mathbf{v}, t)$, which in principle has seven dimensions. Although the Monte Carlo method has been very popular and successful for the solution of the BTE in semiconductor device simulation,^{13,14} several works^{12,15,16} have recently solved the BTE by direct methods. This allows noise-free spatial and temporal resolution of the electron distribution function, which in the Monte Carlo method may be difficult to obtain due to the statistical nature of the approach.

In our model, the electron transport is described by the following one-dimensional BTE¹⁷ within the relaxation time approximation

$$-\frac{eE(x)}{m^*} \frac{\partial f(x, v)}{\partial v} + v \frac{\partial f(x, v)}{\partial x} = -\frac{f(x, v) - f_{LE}(x, v)}{\tau}, \quad (1)$$

where m^* is the effective mass in the parabolic band approximation and where we have assumed that the nonequilibrium electron distribution relaxes to a local equilibrium distribution, $f_{LE}(x, v)$, which we in the following assume to describe non-degenerate statistics according to the following normalized Maxwell-Boltzmann (MB) distribution

$$f_{LE}(x, v) = n(x) \left[\frac{m^*}{2\pi k_B T} \right]^{1/2} \exp \left[-\frac{m^* v^2}{2k_B T} \right], \quad (2)$$

where $n(x)$ is the local electron density, and T is the lattice temperature. The electron density is obtained from the full electron distribution according to

$$n(x) = \int f(x, v) dv. \quad (3)$$

The BTE, eq. (1), is coupled to the Poisson equation through the electric field and electron density. In the following we assume that our system is unipolar and hence, that the Poisson equation is given by

$$\frac{d^2 \phi}{dx^2} = -\frac{dE}{dx} = -e \frac{N_D(x) - n(x)}{\epsilon \epsilon_0}, \quad (4)$$

where $N_D(x)$ is a given inhomogeneous doping distribution profile and ϵ is the dielectric constant.

Equations (1-4) are coupled through the electron density and electric field, and thus, they need to be solved self-consistently. We use a numerical approach based on finite difference and relaxation methods, the details of which can be found in Ref. 12. As boundary conditions, we adopt the following scheme: For the potential, the values at the system boundaries, $x_{l(efl)}$ and $x_{r(ight)}$, are fixed to $\phi(x_l) = V_b$ and $\phi(x_r) = 0$, respectively, corresponding to an externally applied voltage V_b . The electron density is allowed to fluctuate around the system boundaries subject to the condition of global charge neutrality, which is enforced between each successive iteration in the self-consistent Poisson-Boltzmann loop. The size of the highly-doped contacts is chosen to be large enough such that the electron density is constant deep inside the contacts. In addition, the size of the contacts has to be large enough, such that the electric field deep in the contacts is constant, and very low. This allows us to use the analytical, linear response solution to the BTE

$$f(x_{l,r}, v) = f_{LE}(x_{l,r}, v) [1 - vE(x_{l,r})\tau/k_B T], \quad (5)$$

as phase space boundary conditions at $x_{l,r}$, where we use the local equilibrium distribution, $f_{LE}(x_{l,r}, v)$ and local electric field, $E(x_{l,r})$, obtained from the previous numerical solution to the Poisson-Boltzmann iterative loop. At the velocity cut-off in phase space, we choose $f(x, v_{\max}) = f(x, -v_{\max}) = f_{LE}(x, v)$, which is reasonable since, in the calculations, we assume $v_{\max} \geq 30k_B T$. A more detailed description and discussion of our numerical method can be found in Ref. 12.

III. RESULTS AND DISCUSSION

In the following, we will present and discuss our main results. First, we will discuss some basic signatures of quasi-ballistic transport, followed by a study of the crossover between the diffusive and quasi-ballistic regimes of transport. Our model structure consists of a lightly doped region (hereafter called the channel), with doping concentration $N = 10^{19} \text{ m}^{-3}$, sandwiched between two highly doped semiconductor contact regions with doping concentration $N^+ = 10^{23} \text{ m}^{-3}$. We assume that the entire $N^+ - N - N^+$ structure consists of GaAs, and use the appropriate parameters in the calculations (effective mass $m^* = 0.067m_0$, where m_0 is the bare electron mass, and dielectric constant $\epsilon = 13.1$). Unless otherwise indicated, we assume that the lightly doped channel region is 200 nm long. In addition, all of our calculations are performed at $T = 300 \text{ K}$, using a scattering time of $\tau = 0.25 \text{ ps}$, which corresponds to a realistic scattering time due to polar optical phonon scattering.¹⁸ The microscopic effects of an energy-dependent scattering mechanism have been previously studied in Ref. 2.

A. Basic signatures of quasi-ballistic transport

The description of transport in submicron, inhomogeneous semiconductor structures such as the ones described in our paper is a complicated process due to *i)* the size of the system, *ii)* the inhomogeneous field distribution, *iii)* the strongly non-equilibrium and quasi-ballistic nature of the problem, *iv)* the self-consistent feedback between the scattering processes and electrostatics. In the following, we will discuss some general properties of our model $N^+ - N - N^+$ structure, which are valid for a wide range of ultrasmall, inhomogeneous semiconductor structures and devices. Some of these results have been previously discussed by us in Ref. 2.

In Fig. 1(a) the electron potential energy (solid line) and electric field (dotted line) are shown for a $N^+ - N - N^+$ structure with dimensions $2.9/0.2/2.9 \mu\text{m}$, for an applied bias voltage of $V_b = -0.3 \text{ V}$. The potential energy has a very slow spatial dependence in the large contacts resulting in only $\approx 50\%$ of the voltage drop occurring within the contact regions. In contrast, most of the potential drops over the lightly doped, deep submicron channel region, resulting in a dramatic spatial variation. Correspondingly, a large field build-up, with opposite sign, occurs at the N^+/N interfaces, a strongly inhomogeneous electric field is observed in the channel region, and in contrast, the field in the contacts is very small and constant, thus validating the assumption of a near-equilibrium solution to the BTE at the system boundaries. The observed strong spatial dependence of the electron potential energy and electric field in the channel region is due to the carrier diffusion induced by the large variation in doping concentration.²

In addition to the electrostatic picture discussed above,

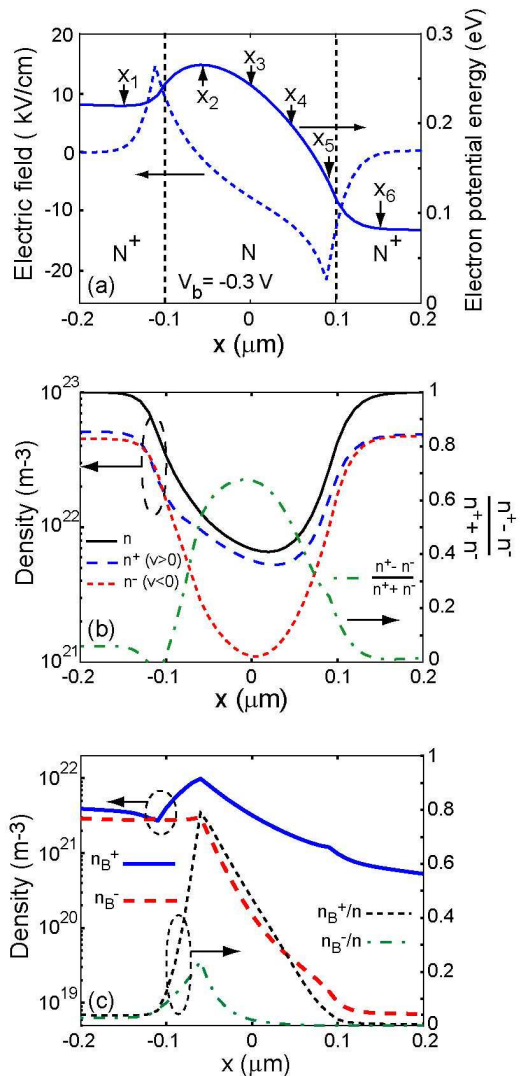


FIG. 1: (Color online) (a) Electron potential energy and electric field for a $N^+ - N - N^+$ structure with doping $10^{23}/10^{19}/10^{23} \text{ m}^{-3}$ for an applied bias voltage of $V_b = -0.3 \text{ V}$, temperature $T = 300 \text{ K}$, and with scattering time $\tau = 2.5 \cdot 10^{-13} \text{ s}$. Vertical dashed lines mark the interfaces between the highly doped N^+ and lightly doped N regions. (b) Electron densities, n^+ , n^- , n , and $(n^+ - n^-)/(n^+ + n^-)$ as defined in the text. (c) “Ballistic” electron densities, n_B^+ , n_B^- , and “ballistic” electron fractions, n_B^+/n , and n_B^-/n as defined in the text.

valuable information can be obtained from the carrier distribution within the system for a given applied external field and inhomogeneous doping profile. In this context, it is interesting to study the separate contributions, n^+ due to electrons with $v \geq 0$ (hereafter denoted as v^+), and n^- due to electrons with $v < 0$ (hereafter denoted as v^-), to the total electron density

$$n(x) = n^+(x) + n^-(x) = \int_{v^+} f(x, v) dv + \int_{v^-} f(x, v) dv. \quad (6)$$

In addition we also introduce and study the “ballistic” electron density,

$$n_B(x) = \int_{|v|>v_p} f(x, v) dv, \quad (7)$$

which corresponds to the density of electrons with energies higher than the top of the potential barrier between the source contact and the channel [occurring at x_2 in Fig. 1(a)], thus corresponding to a “ballistic” electron density. In eq. (7), $v_p = \sqrt{2/m^*[U_0 - U(x)]}$ and U_0 and $U(x)$ are the barrier top and local electron potential energies, obtained from the Poisson equation (4), respectively.

In Fig. 1(b) the electron densities n^+ (dashed line), n^- (dotted line), and $n = n^+ + n^-$ (solid line), i.e., the total electron density, are shown for the structure with the same parameters as discussed in Fig. 1(a). In addition, we show the spatial dependence of the surplus of electrons with velocities v^+ relative to the total electron density, $P_n = (n^+ - n^-)/(n^+ + n^-)$ (dashed-dotted line), which can be viewed as a “polarization” of the electrons in velocity space.

Several observations are made: First, the total electron density, n , displays an asymmetric spatial dependence with respect to the direction of transport, indicating a pile-up of charge at the source-channel interface. Second, it is seen that the difference between the two densities, $n^+ - n^-$, has a significant spatial dependence, and that the minimum of the electron density components occurs at different points along the channel. Furthermore, P_n attains its maximum around mid-channel.

One can view the above results within the following intuitive picture: As electrons are injected from the source contact into the channel, they scatter at a rate given by $1/\tau$. However, the mean free path of the v^+ and v^- electrons is significantly different due to the large built-in electric fields around the channel region, giving rise to a considerable enhancement of the n^+ component of the density in comparison to the n^- . The latter on the contrary is suppressed since, *i*) electrons injected from the drain have to overcome a large potential barrier, *ii*) source-injected electrons scattered from the n^+ contribution and back to the n^- contribution of the density have a relatively short mean free path due to the built-in field that exerts a force in the opposite direction and thus, quickly scatter back to the n^+ component. The spatial dependence of n^+ , n^- , and $(n^+ - n^-)/(n^+ + n^-)$ indicates that the efficiency of the scattering is non-uniform within the channel.

It is interesting to analyze the previously defined “ballistic” electron density, n_B , and compare with the above shown results for the electron densities calculated from the entire velocity range. In Fig. 1(c) the thick solid and dashed lines correspond to the v^+ , and v^- components (which we in the following denote by n_B^+ and n_B^-) of n_B , respectively. In addition, we also show the “ballistic” electron fractions n_B^+/n (thin dotted line), and n_B^-/n (dashed-dotted line).

To the left of the source-channel interface at $x = -0.1 \mu\text{m}$, the two components, n_B^+ and n_B^- , have a slow spatial dependence and are only slightly different in value, reflecting the small field that is present in the source region. Around $x = x_2$, corresponding to the top of the potential barrier [see Fig. 1(a)], the two components rapidly split, and n_B^+ peaks at the barrier top, as expected by the pile-up of source-electrons at the interface, where interestingly, only $\approx 80\%$ of the total density consists of electrons with positive velocity as seen in n_B^+/n . Since the potential barrier seen by the drain-injected electrons from the right is far too large compared to $k_B T$ to explain the large n_B^- component at x_2 in terms of thermionically injected electrons from the drain, the main contribution to that component consists of backscattered source injected electrons. This is consistent with the interesting analyses by Sano^{3,4} in which it was shown mathematically that, due to the singular nature of the BTE (note, that the analyses was made for the BTE in the relaxation time approximation), a finite n_B^- around the top of the barrier separating the source and the channel region, is always present provided there is a finite scattering rate. The intuitive physical picture is that, electrons close to the conduction band edge can have an infinitely small velocity, and thus can spend long enough time to experience a scattering event. If electrons incident from the source experience a sharp potential rise around the barrier, electrons pile up close to the conduction band edge and are successively slowed down, thus increasing the time spent around the barrier region, and correspondingly giving rise to a significant contribution in n_B^- . The contribution to n^- becomes larger the larger the curvature of the potential energy around the barrier region.⁴

Beyond the location of the top of the barrier, for $x > x_2$, n_B^- drops rapidly within the channel region, followed by a change in the slope past the channel-drain interface. The positive component, n_B^+ , on the other hand, has a much slower decay within the channel region, followed by a similar change of decay rate at the channel-drain interface as seen in n_B^- . We note that n_B^+ is two orders of magnitude larger than n_B^- at the channel-drain interface showing that, indeed there are very few drain-injected electrons at kinetic energies comparable to the potential barrier at the source-channel interface.

A simple exponential fit to n_B^+ and n_B^- in the channel region shows that the mean free paths of electrons with $v > 0$ and $v < 0$ are ≈ 140 and 50 nm, respectively. Hence, source-injected electrons have a mean free path comparable to the channel region and, thus, propagate quasi-ballistically. However, inspite of the quasi-ballistic transport of these electrons, their relative contribution to the total electron density in the drain is very small, as shown by the thin dashed and thin dashed-dotted line representing n_B^+/n and n_B^-/n in Fig. 1(c). As expected, the fractions n_B^+/n and n_B^-/n reach their maximum at the barrier top and subsequently decrease monotonically in the channel. We note, however, that n_B^-/n has an exponential-like decay rate, indicative of diffusive-

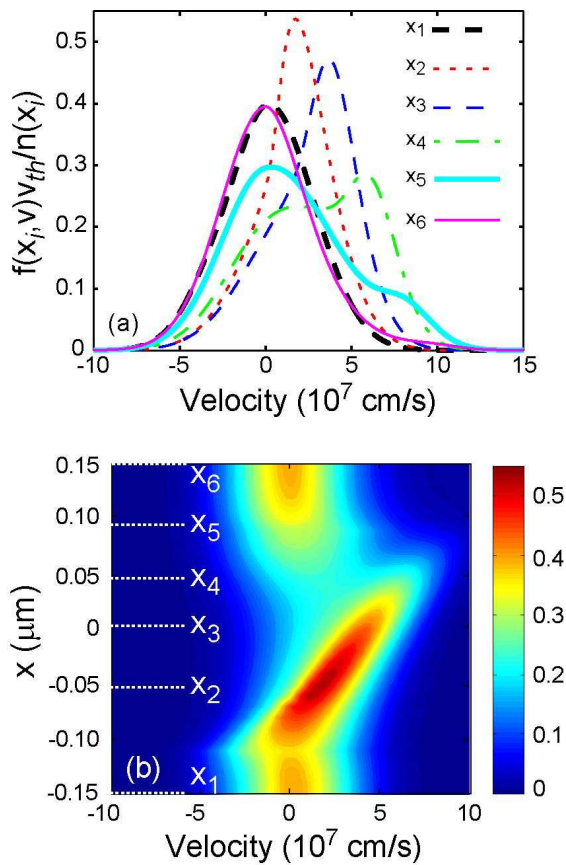


FIG. 2: (Color online) (a) Normalized electron distribution, $f(x_i, v)v_{th}/n(x_i)$, for the structure studied in Fig. 1, calculated at the spatial points x_1 - x_6 as marked by the arrows in Figs. 1(a) and 2(b), for $V_b = -0.3$ V. (b) Contour plot of $f(x, v)v_{th}/n(x)$ around the lightly doped N region.

like transport, in contrast to n_B^+/n which decays almost linearly.

Full information about the microscopic details of the electron transport is contained in the nonequilibrium electron distribution function, to which we have access through our self-consistent solution of the BTE. In Fig. 2(a) we show the normalized electron distribution function, $f(x_i, v)v_{th}/n(x_i)$, where v_{th} is the thermal velocity and $n(x_i)$ is the electron density at x_i , calculated at different locations: one point in the source contact, four points along the channel region, and one point in the drain contact [same as arrows in Fig. 1(a)]. The electron distribution shows a strong spatial dependence, and a far-from-equilibrium form at all but two of the spatial points depicted in Fig. 2(a), namely the ones in the contacts. The thick dashed curve, corresponding to the distribution at $x_1 = -0.15 \mu\text{m}$, is nearly Maxwellian, showing that the electrons at that point are near equilibrium. This is in agreement with the fact that x_1 is situated in the contact region, where the field is very small and constant [see Figs. 1(a) and 2(b)] and thus, the electrons are distributed according to a shifted MB

distribution, as given by the linear response solution to the BTE, eq. (5).

The electron distributions at x_2 - x_5 on the other hand are highly asymmetric, displaying a strong weight toward positive velocities, as well as pronounced structure in the high-velocity tail for v^+ . At $x_2 = -0.05 \mu\text{m}$, the dotted curve shows the electron distribution at the top of the potential barrier between the source and channel regions. The distribution is distorted from a Gaussian-like MB distribution and shows a suppression of electrons in the $v < 0$ tail of the distribution as expected since, intuitively, only electrons injected from the source, with positive velocities, should be present. The presence of a negative-velocity tail in the distribution at the top of the potential barrier is again in accordance with our discussion above and the findings of Sano,^{3,4} showing that significant backscattering occurs around the barrier region due to the sharp potential barrier and corresponding pile-up of electrons at the conduction band edge resulting in an increased backscattering efficiency due to the prolonged dwell time in the barrier vicinity.

Beyond the barrier top, the peak of the distribution rapidly shifts toward higher velocities and is significantly broadened ($x_3 = 0$). In addition, beyond the channel half-point, the low-velocity contribution of the distribution function increases, and a second peak emerges, as seen in the dash-dotted line, corresponding to $x_4 = 0.05 \mu\text{m}$. At $x_5 = 0.09 \mu\text{m}$, the low-velocity peak dominates and only a shoulder is observed on the high-velocity side of the non-equilibrium distribution. Finally, at $x_6 = 0.15 \mu\text{m}$, i.e., in the drain contact, the distribution function again assumes a near-equilibrium form. Note however that a high-velocity tail is still observable, and the distribution function, although closely resembling a shifted MB distribution, is significantly different from the one at x_1 .

A contour plot of $f(x, v)v_{th}/n(x)$ around the channel region is shown in Fig. 2(b) and further illustrates the general features. The emergence of a narrow peak and its rapid shift toward high velocities for $x > x_2$ are clearly seen. The horizontal lines indicate the points x_1 - x_6 corresponding to the curves in Fig. 2(a) and the arrows in the potential energy in Fig. 1(a).

The observed features are a signature of *quasi-ballistic transport*. The high-velocity peak in the distribution corresponds to *ballistic* electrons which, initially injected over the source-channel barrier, due to the rapid and large (compared to $k_B T$) potential drop and correspond-

ing strong inhomogeneous electric field, are accelerated to high (positive) velocities. As discussed before, in the process, the mean free path of backscattered electrons is strongly reduced by the large electric field, and thus, the “ballistic” peak reaches very high velocities, and penetrates deep into the channel region, as seen in Figs. 2(a) and 2(b). However, in addition to the narrow “ballistic” peak, a broad distribution of electrons occupy the low and negative velocity part of the phase space. This com-

ponent of the distribution function becomes more and more pronounced beyond the channel mid-point. The origin of this broadening at the drain end of the channel is due to electrons with $v < 0$, injected from a near-equilibrium distribution in the drain contact which penetrate the channel and contribute to the negative and low velocity components of the distribution function. Within the channel, the inhomogeneous electric field causes a non-uniform dependence of the mean free paths of the n^+ and n^- components of the electron density, as discussed previously, which in turn creates a feedback to the electrostatics due to the charge (re)distribution. It is thus evident from Figs. 2(a) and 2(b) that the microscopic details of the influence of scattering in a submicron channel can be obtained only from the full non-equilibrium distribution function, which can only be obtained by the self-consistent solution of the BTE.

B. Crossover between quasi-ballistic and diffusive transport

In the following, we will discuss the crossover between the quasi-ballistic and diffusive regimes of transport in terms of numerical calculations and a study of the microscopic signatures discussed above. We will focus on the quantities discussed in the previous section and investigate their dependence on an externally applied bias voltage, as well as the dependence on the channel length. We have performed calculations for different structures with channel lengths ranging between 0.2 to 4 μm . In order to exclude the influence of finite contact size on the results, we have performed and compared studies using two definitions of the channel length variations. In one case, which we simply call the constant contact (CC) size case, we keep the size of the contacts fixed, while varying the channel length, thus effectively changing the total sample size. The second case, which we simply call the constant sample (CS) size case, we assume that the total sample size is constant, such that the variation of the channel length effectively reduces the contact size. In both cases, as will be seen in the presented results, the contact sizes are found to be large enough not to influence the main features of our study.

1. Electrostatics

In Figs. 3, we show our calculated results of the electrostatics for different applied bias voltages and different channel lengths. In Fig. 3(a), the potential energy profiles (thin lines) and electric field distributions (thick lines) are shown for an $N^+/N/N^+$ structure with dimensions 2.9/0.2/2.9 μm and the same parameters used in the previous results, calculated at the applied bias voltages $V_b = 0, -0.1, -0.2, -0.3$ V. Even in the absence of an externally applied field, a large potential barrier and a corresponding strong and inhomogeneous electric field

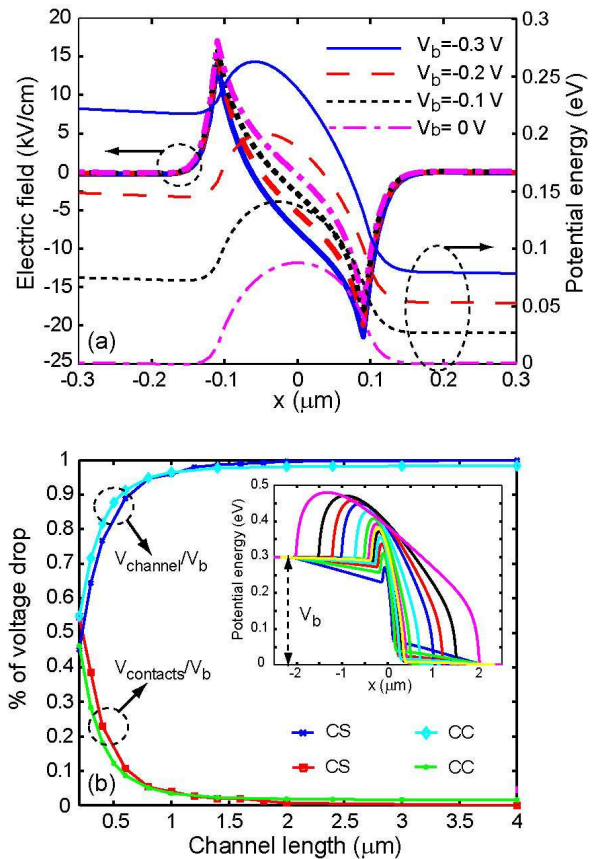


FIG. 3: (Color online) (a) Potential energy (thin lines) and electric field (thick lines) profiles for different external bias voltages, for the same parameters and structure studied in Figs. 1 and 2. (b) Fraction of the potential drop that occurs across the contacts, V_{contacts}/V_b , and the channel, V_{channel}/V_b , as a function of channel length. Inset shows the spatial dependence of the potential energy profile for channel lengths in the range $L_c = 0.2 - 4$ μm . The different curves correspond to the constant contact (CC) and constant sample (CS) size approaches to the channel length variation in the calculations.

builds up in the channel region due to the interdiffusion of electrons from the highly doped contact regions to the lightly doped channel region. As an external bias is applied to the sample boundaries at ± 3 μm , the majority of the potential drops over the channel region. We note that, for the considered bias range, $V_b = -0.1$ to -0.3 V, the fraction of the potential drop that takes place over the channel region is effectively the same and $\approx 50\%$. The electric field, although varying with the same range of ≈ -25 to ≈ 15 kV/cm has an increasingly stronger spatial dependence with increasing bias voltage.

To investigate the crossover between the diffusive and quasi-ballistic regimes of transport in the electrostatics, we have studied the electrostatic response for structures with different channel lengths, ranging between $L_c = 0.2$ and 4 μm . The potential energy profiles for different

channel lengths (calculated for the CS case) at $V_b = -0.3$ V are shown in the inset of Fig. 3(b). It is evident from the results that, although most of the potential drop, and hence resistance, occurs over the channel region, the fraction of the potential drop associated with the channel region strongly depends on the channel length.

In Fig. 3(b) we show the fraction of the potential drop that occurs across the channel, $V_{channel}/V_b$, and contact, $V_{contacts}/V_b$, regions, respectively, for different channel lengths. For long channels, virtually all of the applied voltage drops across the channel region, irrespectively of the magnitude of the applied voltage (comparison of the results calculated for bias voltages in the range $V_b = -0.3$ to $V_b = -0.1$ V show that there are very small variations in the length dependence and magnitude of the voltage distribution in the system, within the considered range of bias voltage). However, as the channel length is successively decreased below $\approx 1.5 \mu\text{m}$, the fraction $V_{channel}/V_b$ gradually decreases, while $V_{contacts}/V_b$ gradually increases, to the point where, for $L_c < 0.3 \mu\text{m}$, the majority of the potential drop occurs across the contact regions. Note that the calculated curves for the CC and CS size cases are almost identical, showing that no contact size effects are responsible for the observed features.

The observed results and dependence of $V_{channel}/V_b$ and $V_{contacts}/V_b$ show that a crossover occurs around $L_c \approx 1.5 \mu\text{m}$ and that for shorter channel lengths, ballistic effects become important. With decreasing channel length, the transfer of the voltage drop from the channel region to the contact regions, indicates that the transport becomes increasingly ballistic and it is expected that for very short channels, the majority of the voltage drop will occur across the contact regions, and only a very small (but finite) resistance will occur within the channel region. The observed features in the electrostatic response are a *signature of the crossover between the diffusive and quasi-ballistic regimes of transport*.

2. Electron density

Next, we perform a similar study of the electron densities n^+ and n^- , defined earlier in the text. In Fig. 4(a) we show the electron density around the channel region for the same structure as in Fig. 3(a), calculated at the same bias voltages. The thick and thin lines correspond to the n^+ and n^- components of the total density, respectively. At $V_b = 0$ the two components are naturally centered, although slightly shifted from each other, around the channel mid-point. The slight shift is due to the fact that, as seen in Fig. 3(a), the electric field is non-zero everywhere but at mid-channel, and anti-symmetric with respect to the channel center. Hence, the electron distributions in each half of the channel consist of a slightly shifted MB distribution. In the channel half close to the source, the distribution is shifted toward negative velocities, whereas the distribution in the other half is shifted toward positive velocity, see Fig. 6(d) for a contour plot

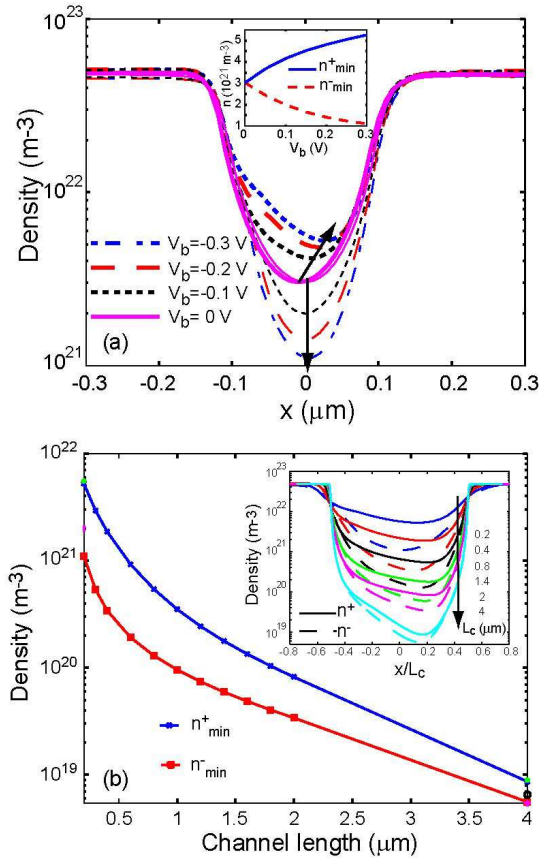


FIG. 4: (Color online) (a) Electron densities, n^+ (thick lines) and n^- (thin lines) for the same structure and bias voltages as in Fig. 3. Inset shows the minimum densities, n_{\min}^+ (solid line) and n_{\min}^- (dashed line) as a function of V_b . (b) Minimum channel densities, n_{\min}^+ and n_{\min}^- , as a function of channel length. Inset shows electron density profiles, n^+ (solid lines) and n^- (dashed lines), as a function of x/L_c , for different channel lengths, L_c .

of the electron distribution around the channel region at zero bias. Consequently, $n^+ - n^- \neq 0$ around the channel region (except at the channel mid-point), where the built-in field is non-zero. Note, however, that the *total* electron density is entirely symmetric along the x -direction (not shown here), as required since $V_b = 0$.

As a bias voltage is applied, two main observations can be made. First, the difference between the two components, $n^+ - n^-$, increases considerably with increasing $|V_b|$, which is also shown in the inset to the figure for the minimum densities, n_{\min}^+ and n_{\min}^- , along the channel. Second, the spatial dependence of n^+ is very different from that of n^- , and more importantly varies considerably for different applied voltages. In particular, the position of n_{\min}^+ changes significantly with V_b , whereas the position of n_{\min}^- is roughly bias independent, as indicated by the schematic lines in the figure. This is an indication that the efficiency of the scattering is different for the v^+ and v^- electrons. Interestingly, the relative excess of

v^+ electrons in the channel region reaches its maximum around mid-channel (not shown), as previously seen in Fig. 1(b) for $V_b = -0.3$ V, and the position is relatively insensitive to the applied bias voltage. This is another indication that the behavior in the channel is controlled by the intrinsic fields and doping profiles rather than the externally applied electric fields.

As the channel length is increased (for $V_b = -0.3$ V) the spatial dependence of the electron densities n^+ and n^- changes significantly. In the inset of Fig. 4(b) we show n^+ (solid lines) and n^- (dashed lines) for different channel lengths ranging between $L_c = 0.2 - 4 \mu\text{m}$, as a function of x/L_c . In addition, Fig. 4(b) shows the dependence of the minimum densities, n_{min}^+ and n_{min}^- as a function of the channel length, calculated at -0.3 V for the CS case (we verified again that the contact size and length scaling scheme do not influence the results qualitatively).

It is seen that: First, as the channel length increases, the electron density in the channel region decreases, approaching the value of the background doping, 10^{19}m^{-3} . Second, the large magnitude difference between n_{min}^+ and n_{min}^- , observed for short channel lengths, decreases. Third, a crossover from a superexponential to an exponential dependence of $n_{\text{min}}^{+(-)}$ on the channel length is observed around $\approx 1.5 \mu\text{m}$. The latter observation we again interpret as a signature of a transition between the quasi-ballistic and diffusive regimes of transport, and occurs around similar channel lengths as observed in the length dependence of the electrostatic response, discussed in Fig. 3(b). For long channel lengths, the density dependence approaches the purely diffusive regime in which the n^+ and n^- have a similar spatial dependence and approach the values of the background doping.

It is interesting to compare the results for the total electron densities, obtained by the integration of the electron distribution over the entire velocity space, see eq. (6), with the “ballistic” electron densities, defined in eq. (7). In Fig. 5 we show the fraction of positive and negative velocity components, n_B^+ and n_B^- , of n_B defined in eq. (7), relative to the total density.

In Fig. 5(a) we show the results for the same 200 nm channel length structure studied in Figs. 1, 2, 3(a), and 4(a), calculated for the bias voltages $V_b = -0.1 - 0.2$ and -0.3 V. With the decrease of bias voltage, the two peaks corresponding to n_B^+/n (thick lines) and n_B^-/n (thin lines) are shifted toward the middle of the channel, and decrease and increase, respectively, as expected by the smaller asymmetry and magnitude of the electric field. We note that, throughout the presented bias voltage range, n_B^+/n decays approximately linearly on both sides of the peak centered at the top of the potential barrier at the source-drain interface. The fraction of negative “ballistic” electrons, n_B^-/n , on the other hand, has a faster, exponential-like decay on the drain side of the potential barrier, indicating diffusive-like transport.

The length dependence of the ballistic fraction of electrons is found to show a distinct signature of the crossover

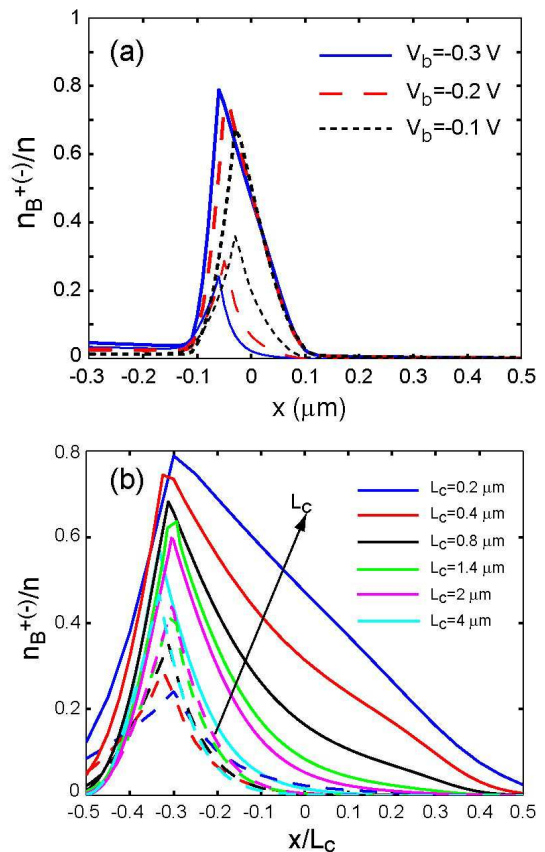


FIG. 5: (Color online) “Ballistic” electron densities, n_B^+ and n_B^- as defined in the text, for (a) the same structure and applied voltages as in Fig. 4(a), and (b) different channel lengths, L_c , vs. relative channel position, x/L_c .

between the diffusive and quasi-ballistic regimes of transport, at similar channel lengths where the crossover was observed in the electrostatic response as well as the total electron density distribution.

In Fig. 5(b), we show n_B^+/n (solid lines) and n_B^-/n (dashed lines) as a function of x/L_c . Interestingly, n_B^-/n has similar decay lengths, relative to L_c , and an almost vanishing contribution around mid-channel (with the exception of the structure with $L_c = 0.2 \mu\text{m}$). We attribute this behavior to the diffusive nature of the transport of electrons with $v < 0$, since the resistance in the diffusive regime is linear with respect to the channel length.

The positive velocity ballistic electron fraction n_B^+/n on the other hand has: *i*) a similar decay length and length dependence with n_B^-/n for $L_c = 4 \mu\text{m}$, *ii*) an increasing relative decay length for decreasing channel length, yielding a significant contribution throughout the full extension of the channel. More importantly, it is interesting to note the transition between an exponential-like dependence for long channel lengths, to an almost linear dependence at shorter channel lengths, as a function of the relative position, x/L_c , within the channel region.

We interpret this as yet another signature of the crossover between the diffusive and quasi-ballistic regimes of transport.

3. Electron distribution function

Having discussed the signatures of the quasi-ballistic and diffusive regimes of transport in the electrostatic response and the electron density distribution we now direct our attention to the full nonequilibrium distribution function. In Figs. 6 we show the calculated normalized distribution function, $f(x, v)v_{th}/n(x)$, for 200 nm channel structures for different applied voltages. Figure 6(a) shows the calculated normalized distribution at $V_b = -0.3$ and is identical to the one shown in Fig. 2(b), and thus displays the previously discussed ballistic, high-velocity peak throughout the channel region. This peak shifts rapidly toward higher velocities along the direction of transport and dominates the distribution function well into the second half of the channel, close to the drain side of the system. In the vicinity of the drain, however, as previously discussed, drain-injected electrons spill over into the channel and dominate the electron distribution. Note however that the two contributions are well separated in phase-space and thus can be easily identified.

As the bias voltage is decreased, the ballistic signatures become less pronounced. Although there still are ballistic peak-like features for $V_b = -0.2$ and -0.1 V, see Figs. 6(b) and (c), respectively, the maximum velocity and the penetration depth of the peak into the channel, i.e., the region in which it dominates the electron distribution, are decreased. Furthermore, a smoother transition occurs between the main peaks in the distribution on the source and drain side of the channel [see Fig. 6(c)] indicating an increasingly diffusive character of the transport. In Fig. 6(d), for $V_b = 0$ V, the distribution is as expected symmetric along the direction of transport, but nevertheless reflects the inhomogeneous properties of the sample, as seen in the slightly shifted distributions around each of the two interfaces.

In Fig. 7 we show the normalized electron distribution functions, calculated at $V_b = -0.3$ V, and for the channel lengths $L_c = 0.2, 0.8, 1.4,$ and $4 \mu\text{m}$. We again include the results for the 200 nm long channel and $V_b = -0.3$ V biased system for comparison in Fig. 7(a) [same as shown in Fig. 2(b) and 6(a)]. Also, for the sake of comparison between the different structures, we show the normalized electron distribution function as a function of velocity, v , and normalized spatial position in the channel, x/L_c .

For $L_c = 0.8 \mu\text{m}$, it is clear that the quasi-ballistic features are persistent, although weaker, i.e., lower maximum velocity and extension into the channel region (relative to the channel length), as well as a smaller separation between the drain- and source-injected electron distributions. Note again that we plot the results against x/L_c and that here, the ballistic peak extends over 300 nm into the channel.

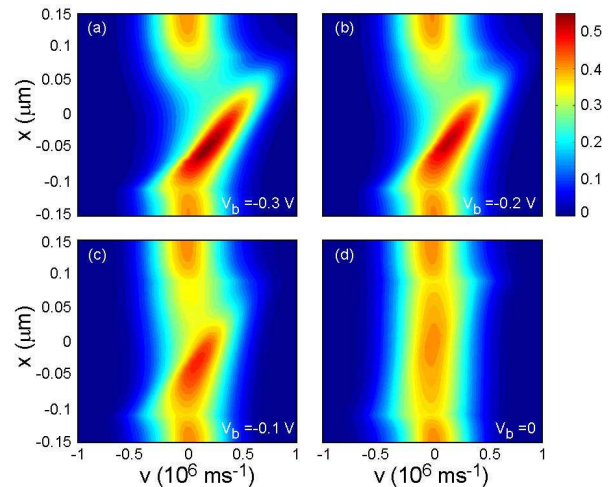


FIG. 6: (Color online) Normalized electron distribution, $f(x, v)v_{th}/n(x)$, for the structure with $L_c = 200$ nm and the same parameters as studied in Figs. 1 and 2, calculated at the bias voltages, (a) $V_b = -0.3$ V, (b) $V_b = -0.2$ V, (c) $V_b = -0.1$ V, and (d) $V = 0$.

For $L_c = 1.4 \mu\text{m}$, the distribution function shows significantly reduced ballistic features. At this channel length, there is no clear formation of a ballistic peak as in the previous cases. Furthermore, the distribution has comparable width, only one dominant peak throughout the entire channel region and a smooth connection between the near-equilibrium source and drain distributions. This indicates that the transport is close-to-diffusive. For longer channels, the electron distribution becomes even more featureless as the transport becomes more and more diffusive. In Fig. 7(d), the distribution function for a $L_c = 4 \mu\text{m}$ channel based system is shown for comparison. No ballistic features are present, the velocities are low in comparison to the previous cases and the distribution in the channel region, although broadened and shifted due to the increased fields, is close to the electron distributions in the source and drain contacts. For channel lengths shorter than $L_c = 1.4 \mu\text{m}$ we have, however, seen a transition toward an increasingly ballistic regime of transport, with features resembling the ones shown in Figs. 7(a) and (b).

IV. SUMMARY AND CONCLUSIONS

In summary, we have performed a detailed microscopic study of quasi-ballistic transport in deep submicron semiconductor channels. In particular, we studied the crossover between the quasi-ballistic and diffusive regimes of transport and identified signatures in the electrostatic response, electron density and full, nonequilibrium electron distribution function, that are due to ballistic transport. The study was performed by numerically solving the coupled, nonequilibrium Boltzmann-Poisson

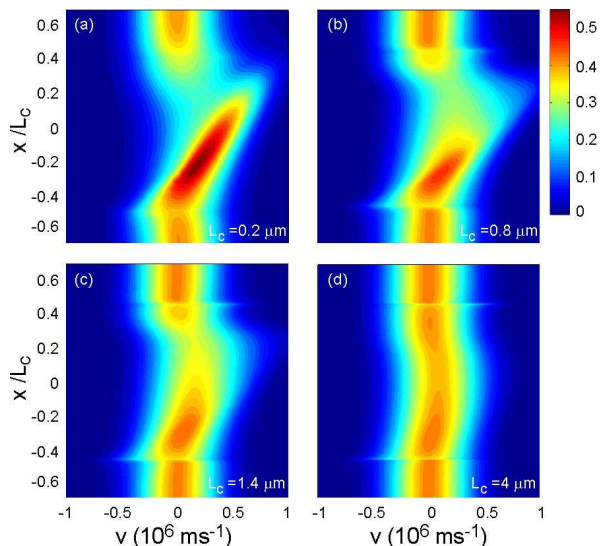


FIG. 7: (Color online) Normalized electron distribution, $f(x, v)v_{th}/n(x)$, for a structure with externally applied bias voltage $V_b = -0.3$ V, calculated for the channel lengths (a) $L_c = 0.2 \mu\text{m}$, (b) $L_c = 0.8 \mu\text{m}$, (c) $L_c = 1.4 \mu\text{m}$, and (d) $L_c = 4 \mu\text{m}$.

system of equations, using a self-consistent direct method developed by us, that enables us to obtain noise-free electron distributions throughout the interesting submicron channel regions.

Semiconductor systems on the deep submicron and nanometer scale can in general very easily be brought out of equilibrium due to their reduced dimensionality. As shown in our model structures, even for moderately downscaled channels and realistic doping levels, the built-in fields are high and have a very strong spatial dependence. Electron transport subject to these fields is therefore highly out-of-equilibrium and drift-diffusion approaches break down.

Our self-consistent calculations of the electron distribution function in submicron GaAs channels using the Boltzmann-Poisson equations show that the electron distribution is radically different from a shifted Maxwell-Boltzmann distribution. The distribution is far from Gaussian-shaped, has a large broadening, and displays pronounced features, peaks and shoulders in the high-velocity tail of the distribution. The high-velocity features are signatures of ballistic transport, which occur due to the large and strongly spatially varying electric fields. The large broadening and significant contribution to the negative-velocity component of the distribution are, however, in part due to backscattered electrons in the channel, and partly due to electrons injected from the drain.

We performed an analysis of the spatial density distributions for electrons with positive and negative velocities, respectively. It was shown that the relative scattering efficiency varies within the channel region and gives

rise to asymmetric density distributions for the forward and backward traveling electrons. We also defined and studied a “ballistic” electron density, corresponding to electrons with total energies higher than the energy of the top of the barrier at the source-channel interface. It was shown that the spatial dependence for the positive and negative velocity contributions to the total “ballistic” density is radically different. This is due to the large difference in the mean free path between the forward and backward traveling electrons caused by the strong built-in electric field. It was shown that a significant number of the source-injected “ballistic” electrons reach the channel-drain interface and propagate into the drain. The relative fraction of ballistic electrons in the drain is, however, very low due to the orders of magnitude higher electron density in the drain contact.

We have shown how these signatures are affected by an externally applied bias voltage, and more importantly by the length of the channel region. The effects of scattering have thereby explicitly been illustrated.

In general, we have found that a crossover between the diffusive and quasi-ballistic regimes of transport for the GaAs structures with the given doping concentrations studied at room temperatures occurs around channel lengths $L_c \approx 1.5 \mu\text{m}$, which is far longer than the mean free path of ≈ 65 nm determined by the thermal velocity, v_{th} . The main parameters that influence this crossover are the effective mass, the scattering time and the details of the doping profile. Hence, a full self-consistent treatment such as ours is needed to accurately model the crossover between the two regimes of transport.

In the electrostatic response we found that the crossover manifests as a redistribution of the voltage drop between the contacts and the channel region. For large channel lengths, the transport is diffusive and the majority of the potential drop occurs across the channel region. For channel lengths smaller than $\approx 1.5 \mu\text{m}$ a monotonic redistribution of the potential drop from the channel region to the contacts occurs, and a crossover between the two fractions occurs around $\approx 0.3 \mu\text{m}$, beyond which, for decreasing channel lengths, the majority of the potential drop occurs across the contact regions.

Similar crossovers were observed in the total and “ballistic” electron density distributions, $n^{(+,-)}$ and $n_B^{(+,-)}$, as well as in the full, nonequilibrium distribution, $f(x, v)$. In particular, we note that the spatial distribution of n_B^+ relative to x/L_c has an increasingly larger decay length and more importantly shows a crossover between an exponential-like to a linear decay rate around channel lengths at which the crossover between the diffusive and quasi-ballistic regimes of transport were observed in the electrostatic response. The spatial distribution of n_B^- , however, has a relatively similar spatial distribution for different channel lengths, relative to L_c , and displays exponential-like decay indicative of diffusive transport. On a microscopic level, we also showed explicitly how the signatures of the crossover manifest in the nonequi-

librium electron distribution, $f(x, v)$.

In general, scattering and quasi-ballistic transport in ultrasmall semiconductor channels exhibit complex features due to the inherent nonlocal nature of the problem. Our study has provided insight into the microscopic signatures of the problem as well as of the crossover between the diffusive and quasi-ballistic regimes of transport. We note that some of the features reported in this paper resemble experimental observations that may be explained within the presented physical picture.

Acknowledgments

This work was supported by the Indiana 21st Century Research and Technology Fund. Numerical calculations were performed using the facilities at the Center for Computational Nanoscience at Ball State University. Furthermore, the authors like to thank Dr. Savas Kaya for fruitful discussions.

* Electronic address: csontos@phy.ohiou.edu

- ¹ S. E. Ralph, and G. J. Wolga, Phys. Rev. B **42**, 1353 (1990); E. D. Grann, S. J. Sheich, K. T. Tsen, O. F. Sankey, S. E. Günc̈er, and D. K. Ferry, Phys. Rev. B **51**, 1631 (1995); K. T. Tsen, D. K. Ferry, J.-S. Wang, C.-H. Huang, and H.-H. Lin, Appl. Phys. Lett. **69**, 3575 (1996); E. D. Grann, K. T. Tsen, D. K. Ferry, A. Salvador, A. Botcharev, and H. Morkoc, Phys. Rev. B **53**, 9838 (1996); W. Liang, K. T. Tsen, D. K. Ferry, K. H. Kim, J. Y. Lin, and H. X. Jiang, Appl. Phys. Lett. **82**, 1413 (2003); W. Liang, K. T. Tsen, D. K. Ferry, H. Lu, W. J. Schaff, Appl. Phys. Lett. **84**, 3681 (2004).
- ² D. Csontos and S.E. Ulloa, Appl. Phys. Lett. **86**, 253 103 (2005).
- ³ N. Sano, Appl. Phys. Lett. **85**, 4208 (2004).
- ⁴ N. Sano, Phys. Rev. Lett. **93**, 246803 (2004).
- ⁵ J.-H. Rhew, Z. Ren, and M. S. Lundstrom, Solid State Electronics **46**, 1899 (2002).
- ⁶ A. Svizhenko, and M. P. Anantram, IEEE Trans. Electron Dev. **50**, 1459 (2003).
- ⁷ A. Rahman, J. Guo, S. Datta, and M. S. Lundstrom, IEEE Trans. Electron Dev. **50**, 1853 (2003).
- ⁸ M. Lundstrom, and Z. Ren, IEEE Trans. Electron Dev. **49**, 133 (2002).
- ⁹ H. U. Baranger, and J. W. Wilkins, Phys. Rev. B **36**, 1487 (1987).
- ¹⁰ H. U. Baranger, and J. W. Wilkins, Phys. Rev. B **30**, 7349 (1984).
- ¹¹ M. V. Fischetti, and S. E. Laux, Phys. Rev. B **38**, 9721 (1988).
- ¹² D. Csontos, and S. E. Ulloa, J. Comp. Electronics **3**, 215 (2004).
- ¹³ C. Jacoboni, and P. Lugli, The Monte Carlo Method for Semiconductor Device Simulation (Springer-Verlag, Wien, 1989).
- ¹⁴ See, e.g., U. Ravaioli, Semicond. Sci. Technol. **13**, 1 (1998), and references therein.
- ¹⁵ A. Majorana, and R. M. Pitadella, J. Comp. Phys. **174**, 649 (2001).
- ¹⁶ J. A. Carrillo et. al., J. Comp. Phys. **184**, 498 (2003).
- ¹⁷ We assume that the electron distribution function can be decoupled into two equilibrium distribution functions in the y and z directions of motion and one distribution function describing the electron motion in the x direction where the electric field drives the electrons far-from-equilibrium.
- ¹⁸ $e^- - e^-$ scattering, while possibly comparable to polar-optical phonon scattering in the n^+ regions, is much weaker in the channel region due to the low doping concentration ($N_D = 10^{13} \text{ cm}^{-3}$) in that region.